Volume 9, Number 5
1009-1963/2000/09(05)/0368-07
CHINESE PHYSICS
May, 2000
© 2000 Chin. Phys. Soc.

SIMULATION OF MULTIPLE FRACTAL AND COMPACT GROWTH OF ULTRA-THIN FILMS ON HEXAGONAL SUBSTRATE*

WANG DAI-MU(王戴木)[a] and WU ZI-QIN(吴自勤)[b]

[a] *Department of Physics, Fuyang Teachers College, Fuyang* 236032, *China*

[b] *Center of Fundamental Physics, University of Science and Technology of China, Hefei* 230026, *China*

(Received 24 November 1999)

The multiple cluster growth of ultra-thin films with different deposition rate and different substrate temperature has been studied by kinetic Monte-Carlo simulation. With increasing diffusion rate along cluster edges (corresponding to an increasing substrate temperature), pattern structures change smoothly from fractal islands, compact islands with random shapes, to regular islands, and the average branch width of clusters increases continuously up to some constant value in the compact island limit. The formation of the multiple fractal and compact clusters can be described quantitatively by multifractal. The results of multifractal analysis show that with pattern change from fractal to compact islands, the Hausdorff dimension D_0, the information dimension D_1, and the correlation dimension D_2 decrease, while the width and height of the multifractal spectra increase.

PACC: 6890; 0540

I. INTRODUCTION

Pattern formation in nonequilibrium dynamical systems has been studied extensively.[1−4] The aggregation of particles to form clusters during growth of ultra-thin film is one aspect of this problem which is of current interest.[5−8] By using scanning tunnelling microscopy (STM), the different patterns such as fractal and compact growth have been investigated. For example, ramified islands are found in the growth of Pt on Pt(111) at low temperatures, and compact islands are observed at higher temperature.[9] It is generally believed that the pattern formation during ultra-thin film growth is mainly controlled by (i) adatom diffusion on the terrace, (ii) adatom diffusion along the cluster edges, and (iii) the lattice geometry of substrate. Considering these factors, some growth simulations have been done to explore the relationship between growth mechanisms and morphology.[6,10−12]

However, as compared with the famous diffusion-limited aggregation (DLA) moldel, the ultra-thin film growth is a rather complex problem, which is related to simultaneous diffusion of particles, random nucleation and mutual effect between neighbouring clusters besides the three factors mentioned above. The complicate effects on the multiple cluster growth are not yet well understood. In this paper, we study the actual processes of multiple cluster growth at different deposition rates and different substrate temperatures by kinetic Monte-Carlo simulation, and analyse quantitatively the influence of different diffusion processes along cluster edges on the pattern structures. In order to characterize the complex distribution of the clusters formed under different growth conditions, we investigate the multifractal behavior of the clusters formation, and find the multifractal parameters that can provide detailed description about the distributions of the clusters.

II. SIMULATION AND RESULTS

For submonolayer coverage, the island morphology is mainly determined by the deposition rate R, the migration rate for monomers on the terrace h_s, and the migration rate of adatoms along island edge h_e. So the deposition interval can be obtained as $W = h_s/R$, and the island shape (fractal or compact) will depend on the ratio h_e/h_s. The diffusion rate is expressed as Arrhenius form $h_i = \nu_i \exp\{-V_i/kT\}$, with the attempt frequency $\nu_i = \nu_s$ or ν_e for terrace or edge diffusion, and the corresponding activation energy $V_i = V_s$ or V_e. The energy barriers for the edge diffusion processes on the hexagonal substrate generally increase with the number of in-layer nearest neighbors. In order to analyse the atomistic process responsible for the formation of fractal and compact clusters, we distinguish between the diffusion processes that can take place at the island edge (see Fig.1) as follows: i) corner diffusion: an adatom starts

* Project supported by the Natural Science Foundation of Auhui Province, China (Grant No. 99047217).

from a site which is laterally one-fold coordinated to the island, i.e., the initial site is an corner, the final coordination can be 1 or 2. ii) step diffusion: the initial site is laterally two-fold coordinated to the island, the final coordination is 2. iii) corner crossing: the initial coordination is 2, and the final coordination is 1. The activation energy corresponding to these edge diffusion processes are $V_e(1)$, $V_e(2)$ and $V_e(c)$, the relevant edge diffusion rates are $h_e(1)$, $h_e(2)$ and $h_e(c)$, respectively. In our simulations the energy barriers are V_s = 0.20eV, $V_e(1)$=0.35eV, $V_e(2)$=0.45eV, and $V_e(c)$=0.55eV. These parameters were chosen from the conditions under which fractal and compact islands have been observed for the aggregation of Pt on Pt(111).[9] Assuming $\nu_s = \nu_e$, we get the ratio h_e/h_s at various substrate temperatures given in Table 1. Other rate processes such as the detachment of atoms from a step or the evaporation of adatom from an island are too slow in the given temperature range and have been ignored. In addition, the asymmetry of the edge diffusion related to the internal physical parameter V_e is also neglected.[11]

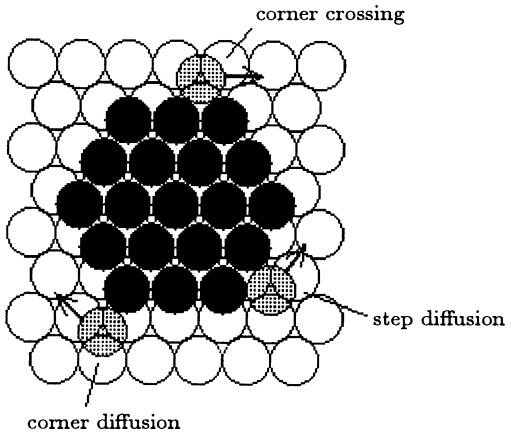


Fig.1. The various edge diffusion processes.

Table 1. Ratio of edge diffusion rate to terrace diffusion rate at various substrate temperatures.

	100K	200K	300K	400K	500K
$h_e(1)/h_s$	2.80×10^{-8}	1.67×10^{-4}	3.04×10^{-3}	1.29×10^{-2}	3.07×10^{-2}
$h_e(2)/h_s$	2.58×10^{-13}	5.05×10^{-7}	6.37×10^{-5}	7.09×10^{-4}	3.03×10^{-3}
$h_e(c)/h_s$	2.38×10^{-18}	1.54×10^{-9}	1.33×10^{-6}	3.94×10^{-5}	2.99×10^{-4}

The simulations were carried out on a hexagonal lattice of 420×420 sites with periodic boundary conditions. At the start, one particle was deposited randomly onto the substrate, and allowed to diffuse along six directions with equal probability to nearest-neighbour sites. When its diffusion steps reached W, the next particle was deposited, and these two particles diffused simultaneously. The W can be regarded as average time interval between successively deposited particles(unit time is taken as one diffusing step on terrace). The procedure was repeated with additional particles which were deposited successively with equal deposition interval W. When two diffusing particles touched, they stopped and became a nucleus. If a diffusing particle moved to a nearest-neighbour site of a cluster, the particle diffused along the cluster edges according to h_e/h_s until it found at least three nearest neighbour particles belonging to the cluster or it was "pinned" in the position by the arrival of one or more additional particles.

In our simulations, the total number of deposited particles was fixed at $N = 30 \times 10^3$ ($\sim$ 0.17 monolayer). Figure 2 shows that the patterns change from fractal to compact with increasing substrate temperature for a deposition interval chosen such that $W = 10 \times 10^3$. When the temperature is 100K, the diffusion along cluster edges is too slow (see Table 1), an adatom arriving at the edge of a cluster does not have time to relax to a more favourable site before it is "pinned" by the arrival of additional particles, the cluster growth is similar to the hit-and-stick DLA molel (Fig.2(a)). When T=200 and 300K, the corner diffusion and step diffusion processes become active while corner crossing is still frozen. With increasing edge diffusion rate, the branches of patterns become thicker(Fig.2(b),(c)). At 400K, the corner crossing process is active, and the growing clusters become compact islands with random shape(Fig.2(d)). When the temperature is high enough (500K), the corner crossing is fast enough, the growth leads to hexagonal islands eventually(Fig.2(e)).

From Table 2 we can see that the number of the clusters decreases with increasing W (decreasing deposition rate). When the deposition rate is high, there are many particles diffusing simultaneously on the substrate, leading to high nucleation rate and large number of clusters. Under the condition of the same deposition rate and the same coverage, the number of clusters in compact growth is larger than that in fractal growth because adatoms in the case of com-

pact growth have larger vacant region to diffuse and larger probability to form a new nucleus. The fractal dimension of individual clusters is measured by sand-box method and averaged from ten clusters selected at randon.

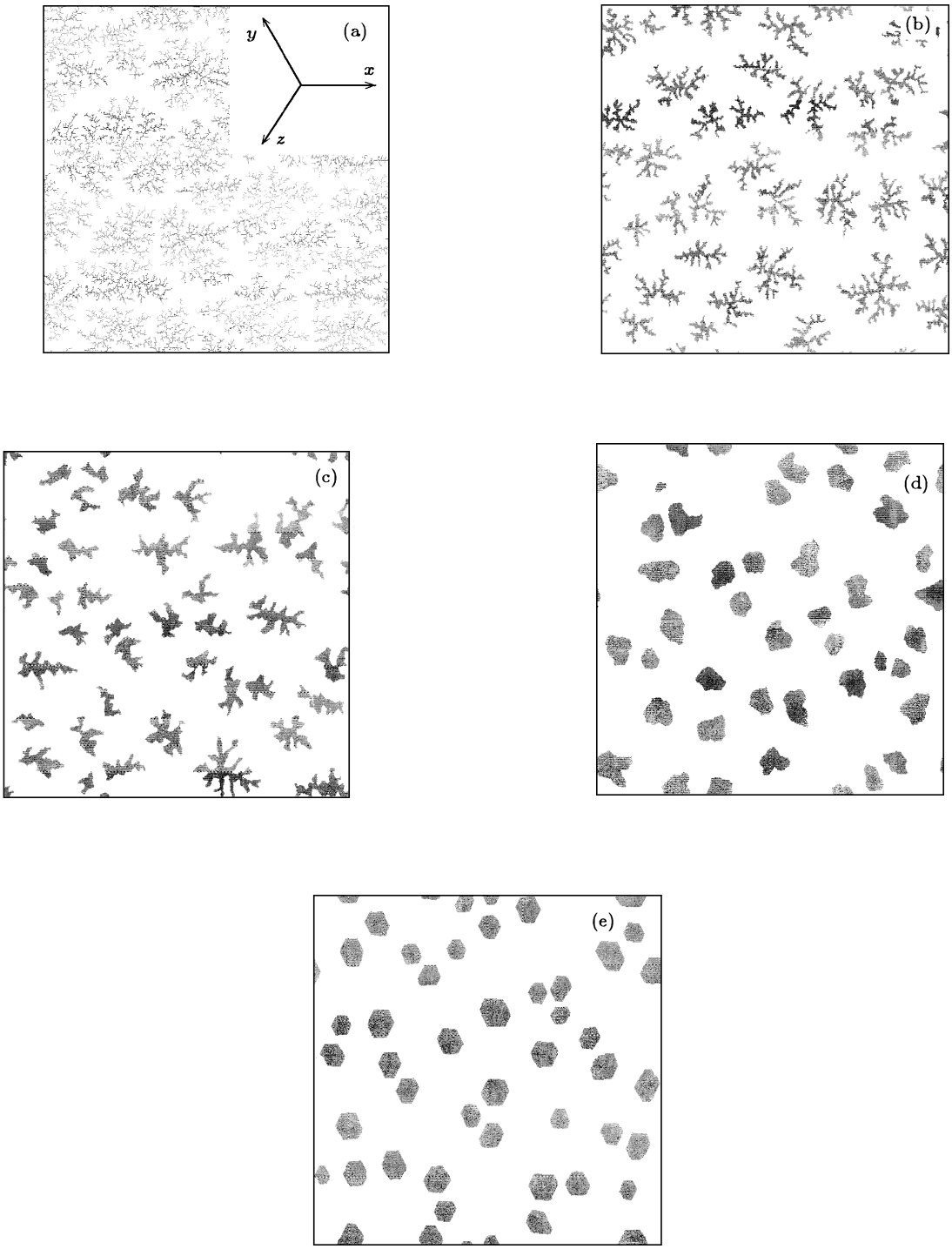


Fig.2. Multiple cluster patterns grown on hexagonal surface lattice with increasing substrate temperature under the condition of $W = 10 \times 10^3$ and $N = 30 \times 10^3$. (a) Fractal growth with the branch width about one atom, in which particle sticks where it hits and does not have time to relax; (b) and (c) fractal growth with increasing branch width, in which edge particles can relax to find two or three nearest neighbours; (d) and (e) compact growth with random and regular shape respectively.

Table 2. Cluster number n, average particle number of a cluster S, average branch width b, and average dimension D for various substrate temperature and various deposition interval.

		100K	150K	200K	250K	300K	350K	400K	450K	500K
$W = 10 \times 10^3$	n	29	33	37	39	41	40	40	42	41
	S	1034	909	811	769	732	750	750	714	732
	b	1.74	3.18	5.71	8.21	11.98	16.31	21.44	22.05	22.08
	D	1.68	1.68	1.71	1.77	1.89	1.93	2.00	2.00	2.00
$W = 3 \times 10^3$	n	49	53	61	65	68	70	74	76	74
	S	612	566	492	462	441	429	405	395	405
	b	1.72	3.24	5.38	7.46	10.13	13.28	15.64	16.14	16.18
	D	1.66	1.67	1.73	1.73	1.88	1.95	2.00	2.00	2.00
$W = 0.5 \times 10^3$	n	110	124	137	148	156	159	164	162	164
	S	273	242	219	203	192	189	183	185	183
	b	1.72	3.01	4.78	6.55	8.23	9.45	10.91	11.43	11.46
	D	1.64	1.66	1.69	1.73	1.91	1.96	2.00	2.00	2.00

In order to analyse quantitatively the transition of the patterns, we introduce b to be the average number of continuous atoms of the clusters along three directions of the hexagonal substrate as shown in Fig.2(a):

$$b = (b_x + b_y + b_z)/3, \tag{1}$$

where b_x is the average number of continuous atoms along horizontal direction(x direction) which can be expressed as:

$$b_x = \frac{1}{N_x} \sum_i \sum_j a_{ij}, \tag{2}$$

where N_x is the total number of linear segments of all the islands along x direction, a_{ij} is the number of atoms in the (i, j) linear segments, and b_y and b_z are the average number of continuous atoms along y and z direction respectively. For ramified growth b is the average branch width of the fractal clusters, and for compact growth b is the average size of the compact islands. The values of b at various substrate temperatures and various deposition intervals (for a fixed coverage ($N = 30 \times 10^3$)) are also listed in Table 2. When the temperature is low, the number of branches of the fractal clusters are large, so the average branch width is small. With increasing substrate temperature, the number of branches of the clusters decrease and average branch width increases rapidly. Further increase of the substrate temperature leads to the transition from fractal growth to compact growth, the value of b is close to a saturated value. From Figs.3 and 2, we can see that the transition occurs when the temperature is about 400K for the chosen values of the parameters V_s and V_e. In the compact island cases, the average size of islands b and the average particle number of islands S increase with increasing deposition interval. Figure 4 shows that S and b obey the relation:$S \propto b^2$.

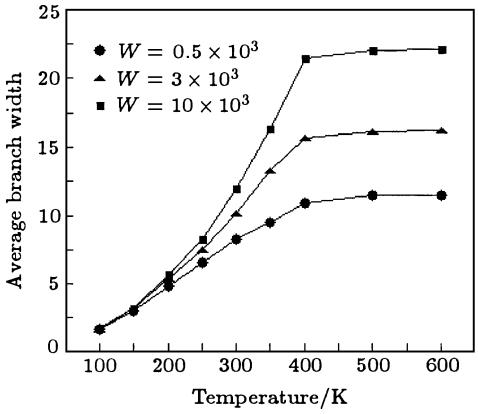


Fig.3. Temperature dependence of the average branch width.

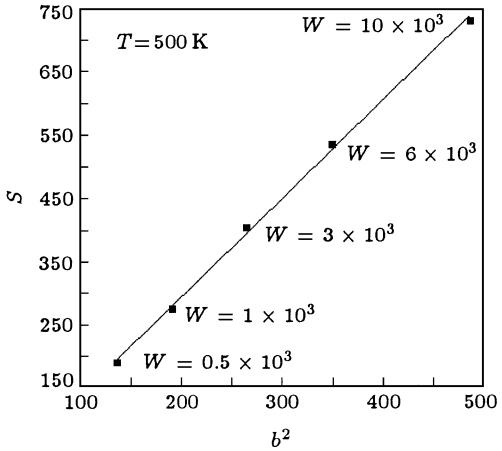


Fig.4. Average particle number S of per cluster vs average branch width.

In Fig.5, b is plotted as a function of coverage for four different temperatures at a fixed deposition interval ($W = 10 \times 10^3$). At low temperature(100K), the edge diffusion is frozen completely, the average branch width of fractals is about 1.7 over the entire deposition process (see Table 3). At high temperature (400K), the growing islands become compact due to the high edge diffusion rate, the average size of islands increases continuously with increasing coverage. At intermediate temperatures, the $b \sim$ coverage curves are composed of two segments, corresponding to the compact growth and ramified growth. In early stage of growth, clusters have compact shape, and branches develop only above certain island size. It can be seen that this island size increases with increasing substrate temperature. During ramified growth (T=200K) the average branch width is nearly constant due to the screening effect of fractal growth, at 300K, the aggregate perimeter is partially screened by the growing tips, b slightly increases with increasing coverage. Figure 5 shows clearly the transition of growth processes from Hit-and-Stick DLA to compact growth with increasing temperature.

Table 3. The average branch width b for various coverage at four different temperatures.

	0.5×10^3	1×10^3	1.5×10^3	2×10^3	4×10^3	6×10^3	8×10^3	10×10^3	14×10^3	20×10^3	30×10^3
100K	1.65	1.65	1.66	1.66	1.71	1.72	1.72	1.73	1.72	1.71	1.73
200K	3.39	3.95	4.23	4.52	5.12	5.36	5.47	5.65	5.66	5.71	5.71
300K	3.17	4.32	5.22	5.76	7.28	8.32	8.99	9.67	10.39	10.88	11.10
400K	3.59	4.73	5.69	6.64	8.81	10.43	11.96	13.04	15.47	18.13	21.39

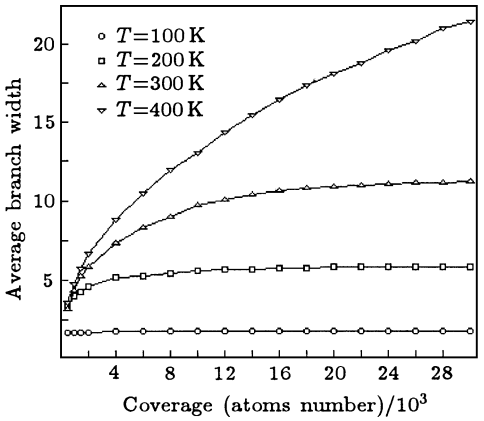


Fig.5. The average branch width vs coverage for four temperatures.

Ⅲ. MULTIFRACTAL ANALYSIS

From Fig.2 we can see that with the change of pattern structures from fractal into compact, the distribution of particles becomes more nonuniform. We can describe quantitatively the distribution by the multifractal approach. By using the box-counting method we can obtain the growth probability as

$$P_{ij}(\varepsilon) = S_{ij}(\varepsilon)/\Sigma S_{ij}(\varepsilon), \tag{3}$$

where $S_{ij}(\varepsilon)$ is the sum of all the particles inside a square box with a size of ε at position (i, j) (let ε=1 when the total lattice of 420×420 sites is taken as the largest box), and $\Sigma S_{ij}(\varepsilon)$ is the summation over all the boxes.

According to their magnitude the total set of probabilities at various ε can be divided into a series of subsets which can be expressed by a power law as

$$P(\varepsilon) \sim \varepsilon^{\alpha}. \tag{4}$$

The number of the boxes $N(\varepsilon)$ with the same probability $P(\varepsilon)$ in any α subset can be expressed as

$$N(\varepsilon) \sim \varepsilon^{-f(\alpha)}. \tag{5}$$

The multifractal spectrum $f(\alpha)$ can be obtained starting from a partition function $\chi_q(\varepsilon)$ defined as

$$\chi_q(\varepsilon) = \sum [P_{ij}(\varepsilon)]^q \sim \varepsilon^{\tau(q)}, \tag{6}$$

where q is the moment order. Figure 6 is the $\ln\chi(q)$-$\ln\varepsilon$ plot when the deposition interval $W = 10 \times 10^3$ and the temperature T=300K. The exponent $\tau(q)$ and the generalized dimension $D(q) = \tau(q)/(q-1)$ can be obtained from the slopes of linear segments I in Fig.6. The linear segments show that the range of scale invariance reaches 2 orders of magnitude.[13] The appearance of the segment Ⅱ is due to the departure from the scale invariance law of the small probabilities.[14−17] The singularity α and function $f(\alpha)$ are obtained by Legendre transformation of q and $\tau(q)$.[14,15]

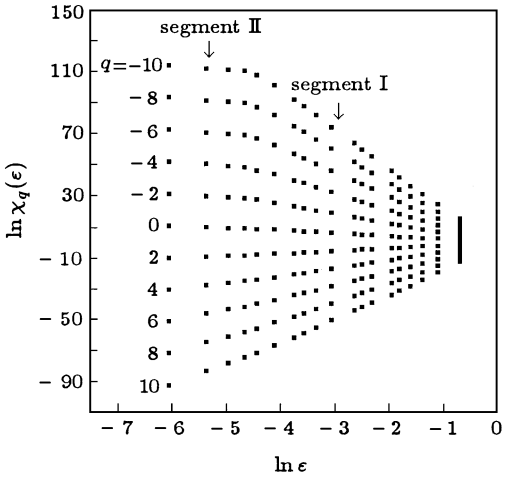


Fig.6. $\ln\chi_q(\varepsilon)$-$\ln\varepsilon$ plots of the probability distribution as $W = 10 \times 10^3$ and T=300K.

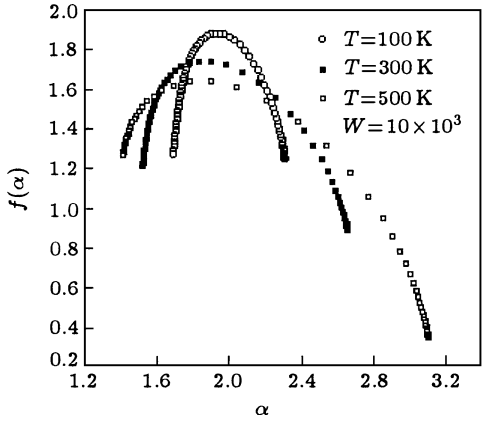


Fig.7. The multifractal spectra of multiple cluster growth in Figs.2(a), 2(c), and 2(e).

Figure 7 presents the multifractal spectra $f(\alpha)$ of the distribution of the growth probability corresponding to Figs.2(a), 2(c), and 2(e). It is evident from Fig.7 that with increasing temperature, the width and height of the spectra increase, while the top $f(\alpha)$ decreases. Table 4 lists the multifractal parameters, where D_0 is the top $f(\alpha)$, i.e., Hausdorff dimension of the nonuniform distribution of the islands, the width of the spectra $\Delta\alpha = \alpha_{\max} - \alpha_{\min}$, the left-side height $\Delta f' = D_0 - f(\alpha_{\min})$, and the right-side height $\Delta f'' = D_0 - f(\alpha_{\max})$. It can be seen that at a fixed deposition interval, D_0, D_1, D_2, $\alpha_{\min}$, and $\Delta f'$ decrease with increasing temperature, while $\alpha_{\max}$, $\Delta\alpha$, and $\Delta f''$ increase; at a fixed temperature, D_0, D_1, D_2 increase with decreasing deposition interval, while $\Delta\alpha$ decreases. When the deposition interval increases and the temperature increases, the number of clusters decreases and the branch width of clusters increases, and the Hausdorff fractal dimension D_0 decreases, because there is larger vacant region between nearby clusters. The information dimension D_1 describes the scaling behavior of entropy of the probability measure.[14] With pattern change from fractal to compact, the parameter D_1 decreases, indicating that the distribution of the islands becomes more irregular and more nonuniform. The minimum singularity $\alpha_{\min}$ and the maximum singularity $\alpha_{\max}$ are connected with the largest and smallest subsets of probability, res-

Table 4. Some multifractal parameters of the growth probability distribution.

W	T/K	D_0	D_1	D_2	$\alpha_{\min}$	$\alpha_{\max}$	$\Delta\alpha$	$f(\alpha_{\min})$	$f(\alpha_{\max})$	$\Delta f'$	$\Delta f''$
	100	1.883	1.834	1.814	1.689	2.308	0.619	1.271	1.251	0.612	0.632
	200	1.789	1.717	1.690	1.528	2.545	1.017	1.258	0.955	0.531	0.834
10×10^3	300	1.744	1.654	1.627	1.517	2.653	1.136	1.215	0.891	0.529	0.853
	400	1.647	1.523	1.489	1.413	3.070	1.657	1.246	0.368	0.401	1.279
	500	1.641	1.516	1.485	1.408	3.100	1.692	1.271	0.354	0.370	1.287
	100	1.902	1.867	1.841	1.677	2.269	0.592	1.312	1.273	0.590	0.629
	200	1.796	1.719	1.705	1.527	2.419	0.892	1.220	1.078	0.576	0.718
3×10^3	300	1.759	1.658	1.640	1.524	2.575	1.051	1.188	1.018	0.571	0.741
	400	1.671	1.602	1.573	1.433	2.901	1.468	1.114	0.573	0.557	1.098
	500	1.667	1.533	1.501	1.427	2.913	1.486	1.115	0.563	0.552	1.104
	100	1.936	1.882	1.857	1.694	2.271	0.577	1.363	1.295	0.573	0.641
	200	1.815	1.724	1.707	1.531	2.349	0.818	1.265	1.143	0.550	0.672
0.5×10^3	300	1.780	1.676	1.648	1.522	2.413	0.891	1.236	1.102	0.544	0.678
	400	1.691	1.603	1.579	1.477	2.658	1.181	1.250	0.829	0.441	0.862
	500	1.684	1.579	1.548	1.453	2.667	1.214	1.248	0.815	0.436	0.869

pectively (Eq.(4)), the wider the range of the bell-shaped or hook-shaped spectra $\Delta\alpha$, the larger the difference between the largest and smallest subsets of probabilities. From Fig.7, it is clear that the difference of the growth probabilities in the case of compact growth is much larger than that in DLA-like growth. $f(\alpha_{\min})$ and $f(\alpha_{\max})$ are the fractal dimensions of the largest subset and smalles subset respectively. According to formula (5), the larger the $f(\alpha)$, the quicker the increase of the number of the boxes $N(\varepsilon)$ in α subset with the decrease of ε. As the temperature increases, the number of branches of the clusters decrease rapidly, the increase of the number of the boxes in the smallest subset of probabilities with decreasing ε becomes slower, leading to an increase of the right-side height of the hook-shaped spectra.

As seen from Fig.6, the $\ln\chi_q$-$\ln\varepsilon$ curves are evidently composed of two segments when $q \leq -1$. Similar phenomena have been observed in the growth probability set of (DLA) cluster[16] and in the secondary electron emission sites on the solid surface and in bulk.[14,15]

IV. CONCLUSION

We have studied the multiple cluster growth of ultra-thin films with fractal and compact morphology on a hexagonal lattice by computer simulation. With increasing substrate temperature, various edge diffusion processes are activated subsequently, and the average branch thickness of clusters increases continuously up to the limiting value corresponding to the average size of compact islands in the compact growth limit. The simulations show the transition from DLA-like growth to compact growth. The nonuniform distribution of the multiple cluster formation shows multifractal behavior, and the multifractal parameters can describe quantitatively the subtle geometrical features of these patterns.

REFERENCES

[1] R. F. Voss, *Phys. Rev.,* **B30**(1984),334.
[2] R.F.Voss,M.Tomkiewicz,*J.Electrochem.Soc.,***132**(1985),371.
[3] P. Meakin, Z. D. Djordjevic, *J. Phys.,* **A19**(1986),2137.
[4] R. Q. Hwang *et al., Phys. Rev. Lett.,* **67**(1991),3279.
[5] Wang Dai-mu, Zhao Ya-dun, Wu Zi-qin,*J. Appl. Phys.,* **71**(1992),5904.
[6] Z. Y. Zhang, X. Chen, M. G. Lagally,*Phys. Rev. Lett.,* **73**(1994),1829.
[7] H. Bruen *et al., Thin Solid Films,* **264**(1995),230.
[8] Z. Y. Zhang, M. G. Lagally, *Science,* **276**(1997),377.
[9] T. Michely *et al., Phys. Rev. Lett.,* **70**(1993),3943.
[10] G.S.Bales,D.C.Chrzan,*Phys.Rev.Lett.,***74**(1995),4879.
[11] M. Hohage *et al., Phys. Rev. Lett.,* **76**(1996),2366.
[12] Wu Feng-min *et al., Chin. Phys. Lett.,* **15**(1998),916.
[13] D. Avnir *et al., Science,* **279**(1998),39.
[14] Li Hua,Ding Ze-jun,Wu Zi-qin,*Phys.Rev.*,**B51**(1995),13554.
[15] Li Hua,Ding Ze-jun,Wu Zi-qin,*Phys.Rev.*,**B53**(1996),16631.
[16] J. Lee, H. E. Stanley, *Phys. Rev. Lett.,* **61**(1988),2945.
[17] Wang Xiao-ping, Wu Zi-qin, *Wuli(Physics)* (in Chinese) (to be published).